Journal of Clinical Trials and Experimental Investigations **2026;5:e21986376**

Original article DOI: 10.5281/zenodo.21986376

Chemosensitizing effects of cromolyn in glioblastoma cells via transglutaminase 2 and ferroptosis signaling

Alp Karaaslan[1], Ceyhan Hacioglu[2*], Burak Ozdemir[1]

[1] Istanbul Sehit Prof. Dr. Ilhan Varank Sancaktepe Training and Research Hospital, Department of Neurosurgery, Istanbul, Türkiye
[2] Duzce University, Faculty of Medicine, Department of Medical Biochemistry, Duzce, Türkiye

Abstract

Objective: Glioblastoma (GBM) remains a therapeutic challenge due to inherent and acquired resistance to temozolomide (TMZ). This study investigated the chemosensitizing potential of cromolyn, a mast cell stabilizer with emerging anti-cancer properties, focusing on its interaction with transglutaminase 2 (TGM2) and ferroptosis signaling.
Materials and methods: We hypothesized that cromolyn could overcome TMZ resistance by inhibiting TGM2 and activating ferroptotic cell death. Using human GBM cell lines (U87, U251, T98G) and a TMZ-resistant derivative (U87-R), we assessed cell viability (CCK-8), clonogenic survival, and protein/gene expression (Western blot, qRT-PCR, ELISA). TGM2 was silenced via siRNA. Ferroptosis was evaluated by measuring lipid peroxidation (C11-BODIPY$^{581/591}$, MDA), GSH, GPX4, and ACSL4 levels. Intracellular labile iron pool and reactive oxygen species were quantified using FerroOrange and dihydroethidium (DHE) staining, respectively.
Results: TGM2 expression was elevated in TMZ-resistant U87-R cells. Cromolyn exhibited time- and concentration-dependent cytotoxicity in both parental and resistant cells, with higher IC_{50} values in the resistant line. Cromolyn treatment downregulated TGM2 expression and, in combination with TMZ, significantly enhanced lipid peroxidation, depleted GSH, suppressed GPX4, and upregulated ACSL4. This was accompanied by increased labile iron and ROS levels. The enhanced cytotoxic effect of TMZ and cromolyn co-treatment was rescued by ferroptosis inhibitors and iron chelation (DFO), but not by apoptosis or necroptosis inhibitors. Furthermore, cromolyn's effect on GPX4 was partially reversed by the proteasome inhibitor MG132. TGM2 silencing similarly sensitized resistant cells to TMZ.
Conclusion: These findings suggest that cromolyn enhances TMZ sensitivity in resistant GBM cells in association with TGM2 modulation and ferroptosis signaling, without establishing TGM2 suppression as the definitive causal mechanism.

Keywords: Cromolyn, glioblastoma, temozolomide, transglutaminase 2.

Correspondence:
Ceyhan Hacioglu, Duzce University, Faculty of Medicine, Department of Medical Biochemistry, Duzce, Türkiye. E-mail: ceyhanhacioglu@duzce.edu.tr

Received: 17 August 2026
Revised: 14 September 2026
Accepted: 22 September 2026
Published: 30 September 2026

ORCID ID of the author(s):
AK: 0000-0003-4213-0906
CH: 0000-0002-0993-6118
BO: 0000-0003-2619-0160

Cite as: Karaaslan A, Hacioglu C, Ozdemir B. Chemosensitizing effects of cromolyn in glioblastoma cells via transglutaminase 2 and ferroptosis signaling. J Clin Trials Exp Investig. 2026;5:e21986376.

2822-5090 /© 2026 Journal of Clinical Trials and Experimental Investigations. Published by Unico's Medicine. This is an open-access article under the terms of the CC BY license (https://creativecommons.org/licenses/by/4.0/).

Introduction

Glioblastoma (GBM), a Grade IV glioma, represents the most common and aggressive primary malignant brain tumor, portending a profoundly unfavorable prognosis with a median survival of merely 12 to 18 months and a five-year survival rate below 10% (1). The current standard of care, which entails maximal safe surgical resection followed by radiotherapy and concomitant temozolomide (TMZ) chemotherapy, provides limited clinical benefit, as tumor recurrence remains almost inevitable (2). This therapeutic failure is largely attributable to the remarkable intra- and inter-tumoral heterogeneity of GBM, which underpins the development of resistance mechanisms (3). These include, but are not limited to, efficient repair of therapy-induced DNA damage, evasion of apoptosis, and the emergence of TMZ resistance, often accompanied by significant adverse effects (4). Consequently, there exists a critical and unmet need to elucidate the molecular pathways driving these resistance phenomena and to develop novel, more effective adjuvant treatment strategies that can circumvent these barriers without augmenting toxicity.

Transglutaminase 2 (TGM2), a multifaceted enzyme possessing both calcium-dependent transamidase and GTPase activities, has emerged as a significant factor in oncogenesis and treatment resistance (5). Its functional repertoire extends to critical physiological processes, including the regulation of efferocytosis—the clearance of apoptotic cells—where it is indispensable for the engulfment phase in macrophages, and its expression is subsequently upregulated in a TGFβ-dependent manner following apoptosis (6). In the context of GBM, TGM2 is preferentially expressed in the mesenchymal subtype and promotes tumor cell proliferation (7). Furthermore, it contributes to therapeutic resistance by facilitating DNA double-strand break repair and modulating p53-mediated responses, thereby protecting cells from radiation- and chemotherapy-induced damage (8). While small-molecule inhibitors targeting TGM2's activities are under development and have shown promise in pre-clinical models, the specific role and source of TGM2 within the complex GBM tumor microenvironment, particularly in immune cells like tumor-associated macrophages (9), remain incompletely elucidated, presenting a critical gap in understanding its full pathophysiological impact.

A promising therapeutic avenue that has emerged to counter such resistance mechanisms is the induction of ferroptosis, an iron-dependent form of regulated cell death driven by the lethal accumulation of lipid peroxides (10). This process stands in contrast to apoptosis and holds particular potential for eliminating therapy-resistant cells, including glioblastoma stem cells, by exploiting their metabolic vulnerabilities (11). The execution of ferroptosis is governed by a complex interplay of metabolic pathways, including the system Xc-/reduced glutathione (GSH)/glutathione peroxidase 4 (GPX4) axis and the enzyme acyl-CoA synthetase long-chain family member 4 (ACSL4), which is critical for propagating lipid peroxidation (12). Notably, ionizing radiation itself can potentiate ferroptosis by upregulating ACSL4, suggesting a synergistic opportunity with standard radiotherapy (13). However, intrinsic resistance, mediated through iron sequestration, antioxidant defenses, and lipid repair systems, often limits its efficacy (14). Intriguingly, preliminary evidence points to a novel role for TGM2 in

modulating ferroptotic sensitivity, as TGM2-knockout models demonstrate a significant resistance to ferroptosis inducers despite unaltered or even pro-ferroptotic basal expression of key markers like ACSL4 and GPX4 (15). This suggests that TGM2 may be a critical and previously unrecognized regulator of the ferroptotic cascade, positioning it as a potential target for overcoming treatment resistance in GBM.

Beyond its canonical role as a mast cell stabilizer, the drug cromolyn has garnered significant interest for its pleiotropic effects in oncology and, more recently, neurobiology (16). Preclinical studies have demonstrated its anti-tumor properties in various cancers, including pancreatic and colon models, through mechanisms involving the inhibition of pro-proliferative pathways and the induction of apoptosis (17,18). Concurrently, cromolyn exhibits a compelling neuroprotective profile, functioning as an inhibitor of amyloid-β aggregation and a modulator of microglial activity by promoting an anti-inflammatory, phagocytic phenotype and suppressing the secretion of key inflammatory cytokines and chemokines (19). These promising actions have propelled cromolyn into clinical trials for neurodegenerative conditions such as Alzheimer's and amyotrophic lateral sclerosis (20). Furthermore, recent investigations have revealed its capacity to dampen pro-fibrotic gene expression in activated microglia and to enhance neurite outgrowth, underscoring its multi-faceted potential in central nervous system pathologies (21). However, despite these advances, a comprehensive understanding of cromolyn's direct effects on cell viability and its precise mechanisms of action within the brain tumor microenvironment remains largely unexplored. In the specific context of GBM, only limited preclinical data are available. To date, no studies have systematically investigated the potential of cromolyn to modulate TMZ resistance or ferroptotic pathways in GBM cells. Given that cromolyn has been shown to cross the blood–brain barrier to some extent in animal models and to exert anti-inflammatory effects on microglia, it represents a candidate repurposable agent that might address both tumor cell-intrinsic resistance and tumor-associated inflammation. Therefore, further mechanistic exploration of cromolyn in GBM is warranted.

Given the emerging understanding of the nexus between TGM2-mediated treatment resistance and ferroptosis in GBM pathogenesis, this study was designed to evaluate the potential of the mast cell stabilizer cromolyn, as a putative TGM2 inhibitor, to augment the cytotoxic efficacy of TMZ by modulating the ferroptotic cell death pathway. We proposed that pharmacological inhibition of TGM2 could sensitize GBM cells to standard chemotherapy by potentiating the ferroptotic cell death pathway. To test this, we systematically evaluated the role of TGM2 in regulating key ferroptosis mediators and lipid peroxidation dynamics in the context of TMZ treatment.

Materials and methods

Cell culture and treatment

The human glioblastoma cell lines U251, U87, and T98G were acquired from the American Type Culture Collection (ATCC). Cells were maintained in high-glucose

Dulbecco's Modified Eagle Medium (DMEM; Sigma-Aldrich) supplemented with 10% fetal bovine serum (FBS; Sigma-Aldrich), 2 mM L-glutamine, and 1% penicillin-streptomycin (10,000 U/mL penicillin and 10 mg/mL streptomycin). Cultures were grown in a humidified incubator at 37°C with 5% CO_2. For routine passaging, cells were rinsed with phosphate-buffered saline (PBS) containing EDTA and subcultured upon reaching approximately 80% confluence. All cell lines were periodically tested and confirmed to be free of mycoplasma contamination.
Cromolyn sodium (C0399; Sigma-Aldrich) was initially dissolved in dimethyl sulfoxide (DMSO; Sigma-Aldrich) to generate a 10 mM master stock solution. Aliquots of this stock were stored at -20°C. For all cell-based assays, the stock solution was subsequently diluted in complete culture medium to achieve the desired final treatment concentrations. The final concentration of DMSO in any treatment condition was rigorously maintained at or below 0.1% (v/v) to preclude solvent-induced cytotoxicity. For all experiments, matched DMSO vehicle controls (≤0.1% v/v) were included and processed in parallel with cromolyn-treated samples. The term 'control' in figure legends refers to vehicle-treated cells.

Establishment of TMZ-resistant experimental cell lines

A TMZ-resistant GBM cell line (designated U87-R) was established from parental U87 GBM cells using a chronic, pulsed selection protocol adapted from our previously established methodology (22). This protocol has been independently validated and reproducibly generates TMZ-resistant derivatives across multiple GBM cell lines. Briefly, cells were subjected to repeated 72 h cycles of exposure to 200 μM TMZ over a continuous three-week period, with the drug-containing medium being refreshed at the initiation of each cycle. This stringent regimen induced substantial cytotoxicity, effectively selecting for a resilient subpopulation capable of survival and proliferation under this selective pressure. The surviving cells were subsequently isolated, expanded, and maintained in culture medium continuously supplemented with 200 μM TMZ to ensure the stability of the resistant phenotype. The resistant population represents a pooled selected population, not a single-cell clone, thereby preserving the heterogeneity of the original parental line. Prior to all experimental procedures, U87-R cells were subjected to a defined washout period of 72 h in TMZ-free complete medium to eliminate residual drug effects and to ensure that observed differences reflect stable acquired resistance rather than acute adaptive responses. Resistance stability was confirmed by maintaining U87-R cells in TMZ-free medium for up to four weeks, followed by re-assessment of TMZ sensitivity.

Transfection

Gene silencing of TGM2 was achieved using a specific small interfering RNA (si-TGM2) and a non-targeting scrambled control sequence, both synthesized by Santa Cruz Biotechnology. The si-TGM2 sequence was 5′-CGC CAG GAC ATG GCA CAA GC-3′. For transfection, cells were seeded in 6-well plates at a density of 1×10^5 cells per well and allowed to adhere. Transfections were performed using Lipofectamine 2000 reagent (Invitrogen) with a final siRNA concentration of 30 nM,

according to the manufacturer's instructions. Following a 6 h incubation period, the transfection medium was replaced with fresh complete culture medium. Cells were then cultured for 48 h at 37°C to allow for maximal gene silencing before being harvested for subsequent experiments.

Cell viability analyses

Cell viability was assessed using the Cell Counting Kit-8 (CCK-8; Cat No: E-CK-A362) according to the manufacturer's instructions. Briefly, cells were seeded into 96-well plates at a density of 1×10^4 cells per well and allowed to adhere for 24 h. Cells were treated with cromolyn (0, 1, 2, 4, 8, 16, and 32 μM) for 12, 24, 48, and 72 hours to assess time- and concentration-dependent effects. Following the respective treatment periods, 100 μL of the CCK-8 reagent was added to each well, and the plates were incubated at 37°C for 60 min. The absorbance of the resulting solution was then measured at a wavelength of 450 nm using a microplate reader.

Biochemical analyses

Following treatment protocols, key ferroptosis-associated biomarkers were quantified using standardized enzyme-linked immunosorbent assay (ELISA) kits. Cells were seeded at a density of 1×10^4 cells per well in 96-well plates and allowed to adhere for 24 h under standard incubator conditions. After the appropriate treatment period, the culture medium was aspirated, and cells were washed twice with ice-cold PBS (pH: 7.4) to remove residual medium components. Cellular lysis was performed directly in the wells using a commercially available ice-cold RIPA lysis buffer (R0278 Sigma-Aldrich), supplemented with a broad-spectrum protease and phosphatase inhibitor cocktail (P2850 Sigma-Aldrich). The lysates were then collected, subjected to vortexing, and clarified by centrifugation at 12,000 × g for 15 min at 4°C. The resulting supernatants were carefully aliquoted and stored at -80°C until analysis. For the specific quantification of malondialdehyde (MDA) and GSH, dedicated colorimetric ELISA kits (MAK085 and MBS727656, respectively) were employed according to the manufacturers' protocols, utilizing the provided standards and controls. MDA was quantified based on its reaction with thiobarbituric acid (TBA) to form a colored adduct measured at 532 nm. GSH was quantified via 5,5′-dithiobis-(2-nitrobenzoic acid) (DTNB)-based reduction, measured at 412 nm. Similarly, the protein levels of GPX4 and ACSL4 were determined using specific quantitative sandwich ELISA kits (MBS2000338 and MBS9331516, respectively). For all assays, an appropriate volume of each sample supernatant was loaded in duplicate wells. After following the prescribed incubation and development steps, the absorbance for each analyte was measured at the respective kit-specified wavelength using a calibrated microplate reader (BioTek Instruments). Final concentrations were calculated by interpolating the mean sample absorbance values against a standard curve generated from the provided reference standards.

Immunofluorescence staining

The cellular localization and expression levels of TGM2 were assessed by immunofluorescence staining. Cultured cells grown in 6-well plates were first fixed with 4% paraformaldehyde in PBS for 20 min at room temperature. Following two thorough washes with PBS, cells were permeabilized by incubation with 0.5% Triton X-100 in PBS for 30 min. Non-specific binding sites were subsequently blocked with a solution of 5% bovine serum albumin (BSA) in PBS for 1 hour at ambient temperature. Cells were then incubated overnight at 4°C with a primary antibody specifically targeting TGM2, diluted in the blocking solution. After extensive washing, samples were incubated for 1 h at room temperature with an appropriate fluorophore-conjugated secondary antibody, protected from light. Cell nuclei were counterstained with 4′,6-diamidino-2-phenylindole (DAPI) for 10 min. Finally, coverslips were mounted onto glass slides using a commercial anti-fade mounting medium. Stained samples were visualized using a laser scanning confocal microscope, and fluorescence intensity was quantified from multiple random fields using ImageJ software.

Assessment of lipid peroxidation via C11-BODIPY$^{581/591}$

Cellular lipid peroxidation was evaluated using the fluorescent probe C11-BODIPY$^{581/591}$ (Thermo Fisher Scientific, D3861). Following experimental treatments, cells were washed with pre-warmed PBS and subsequently loaded with the probe at a final concentration of 2 μM in serum-free culture medium. The incubation was carried out for 30 min at 37°C in a humidified 5% CO_2 incubator, protected from light. After loading, cells were washed twice with PBS to remove excess probe. Fluorescence imaging was performed immediately using a confocal laser scanning microscope. The probe exhibits a spectral shift upon oxidation; the reduced form was excited at 581 nm, and the oxidized form was excited at 488 nm, with respective emissions collected at approximately 591 nm (red channel) and 510 nm (green channel).

Western blot analysis

TGM2 protein expression was evaluated by Western blotting. After treatment, cells were lysed in ice-cold RIPA buffer containing protease inhibitors. Lysates were centrifuged at 14,000 × g for 20 min at 4°C, and protein concentrations were determined using a BCA assay. Equal amounts of protein (20 μg) were separated by 10% SDS-PAGE and transferred to PVDF membranes. Following blocking with 5% BSA, membranes were probed overnight at 4°C with a TGM2-specific primary antibody (2μg/mL, PA5-23219), then with an HRP-conjugated secondary antibody for 1 h at room temperature. Signals were visualized by enhanced chemiluminescence. Membranes were reprobed for β-actin as a loading control. Band intensities were quantified using ImageJ software.

Quantitative real-time PCR (qRT-PCR)

Gene expression levels of GPX4 and ACSL4 were analyzed by qRT-PCR. Following experimental treatments, total RNA was isolated from cultured cells using TRIzol™ Reagent (Thermo Fisher Scientific) according to the manufacturer's protocol. Complementary DNA (cDNA) was synthesized from 1 μg of total RNA using a commercial reverse transcription kit (Applied Biosystems), following the provided instructions. Quantitative PCR amplification was performed using a SYBR™ Green PCR Master Mix (Applied Biosystems) on a StepOnePlus™ Real-Time PCR System (Thermo Fisher Scientific). The reaction mixture contained the prepared cDNA template, gene-specific primers, and the master mix in a final volume of 20 μL. The thermal cycling conditions were as follows: an initial denaturation at 95 °C for 10 min, followed by 40 cycles of denaturation at 95 °C for 15 seconds, and a combined annealing/extension step at 60 °C for 1 min. A dissociation curve analysis was included at the end of each run to confirm the specificity of the amplification. The sequences of the gene-specific primers used were as follows: GPX4: Forward 5′-AAC AGC CCT GTG CTA ATG TGT-3′, Reverse 5′-GCA AAT TCC TTG GAG TGT CCT-3′ ACSL4: Forward 5′-GCC ATC AAG GAG TTC ACC AAG-3′, Reverse 5′-CAG GTA GGC ATC AGG GAA ACA-3′ β actin (internal control): Forward 5′-GGA GCG AGA TCC CTC CAA AAT-3′, Reverse 5′-GGC TGT TGT CAT ACT TCT CAT GG-3′. Relative mRNA expression levels for each target gene were calculated using the comparative $2^{-\Delta\Delta Ct}$ method, normalized to the endogenous control β actin, and expressed as fold change relative to the untreated control group.

Assessment of labile iron pool via FerroOrange staining

The intracellular labile iron pool was detected using the fluorescent probe FerroOrange. Cells were seeded in 6-well plates at a density of 1×10^4 cells per well in complete culture medium and allowed to adhere overnight. After treatment, cells were washed with PBS and subsequently incubated with FerroOrange at a working dilution of 1:1000 in serum-free medium for 30 min at 37°C in the dark. Following incubation, cells were washed three times with PBS to remove residual probe. Fluorescence was immediately visualized and quantified using a fluorescence microscope equipped with appropriate filter sets. Fluorescence intensity, corresponding to labile iron levels, was analyzed from multiple random fields using ImageJ software.

Quantification of intracellular reactive oxygen species (ROS)

Intracellular superoxide anion (O_2^-) levels were measured using the fluorescent probe dihydroethidium (DHE; Sigma-Aldrich, #37291). After treatment, cells were washed with PBS and incubated with 10 μM DHE in serum-free medium for 30 min at 37°C in the dark. Following probe removal and washing, fluorescence was captured immediately using a laser scanning confocal microscope (Olympus). ImageJ software was used to quantify the mean fluorescence intensity, and results are expressed as fold-change relative to untreated controls.

Statistical analysis

Data were presented as mean ± SEM from at least seven independent biological experiments (n = 7). Statistical analyses were conducted using GraphPad Prism 8. Statistical significance was determined by one and two-way ANOVA followed by Tukey's post hoc test. Two-group comparisons were analyzed using unpaired Student's t-test. A p-value <0.05 was considered statistically significant.

Results

TGM2-mediated regulation of TMZ resistance in GBM

Initial screening of three glioma cell lines revealed differential basal expression of TGM2, with the U87 line demonstrating the highest levels, as determined by immunofluorescence and western blot analyses (Figures 1A and 1B). Consequently, this cell line was selected for subsequent resistance studies. Comparative analysis between TMZ-resistant U87 (U87-R) cells and their parental counterparts showed a significant 42% upregulation of TGM2 expression in the resistant population (Figures 1C), demonstrating an association between elevated TGM2 expression and the acquired resistant phenotype. To functionally validate this association, we performed TGM2 silencing in U87-R cells and assessed their response to TMZ (Figures 1D). Following a 24 h treatment with 200 μM TMZ, TGM2 knockdown resulted in a marked increase in cell death (Figures 1E). These collective findings indicate that TGM2 expression is elevated in TMZ-resistant cells and that its suppression re-sensitizes them to chemotherapy, demonstrating a functional association between TGM2 and TMZ resistance in GBM. However, whether TGM2 suppression is the causal mechanism through which cromolyn promotes ferroptosis requires further investigation.

To quantitatively validate the resistant phenotype, we performed TMZ dose-response curves in parental U87 and U87-R cells. The IC_{50} values for TMZ were calculated at 48.3 μM (95% CI: 41.2–56.7 μM) for parental U87 cells and 287.6 μM (95% CI: 251.3–329.1 μM) for U87-R cells, yielding a resistance index (RI) of 5.95.

Cromolyn exhibits time- and concentration-dependent cytotoxicity in both parental and TMZ-resistant GBM cells

The antiproliferative efficacy of cromolyn was systematically evaluated against both TMZ-sensitive parental (U87) and TMZ-resistant (U87-R) GBM cells through a comprehensive concentration- and time-response analysis. To investigate early cellular responses to cromolyn treatment, we first evaluated cell viability at the 12 h time point across a concentration range of 1–32 μM in both parental U87 and TMZ-resistant U87-R cells (Figure 2A–B). At this early exposure duration, cromolyn did not induce a statistically significant reduction in cell viability in either cell line compared to untreated controls ($p > 0.05$). For U87 cells at 12 hours, viability ranged from 98.2% ± 3.1% (1 μM) to 95.7% ± 4.2% (32 μM) relative to control, with no significant differences ($p = 0.34$ to $p = 0.78$). Similarly, in U87-R cells, viability ranged from 97.5% ± 3.8% to 95.9% ± 4.2% ($p = 0.29$ to $p = 0.61$).

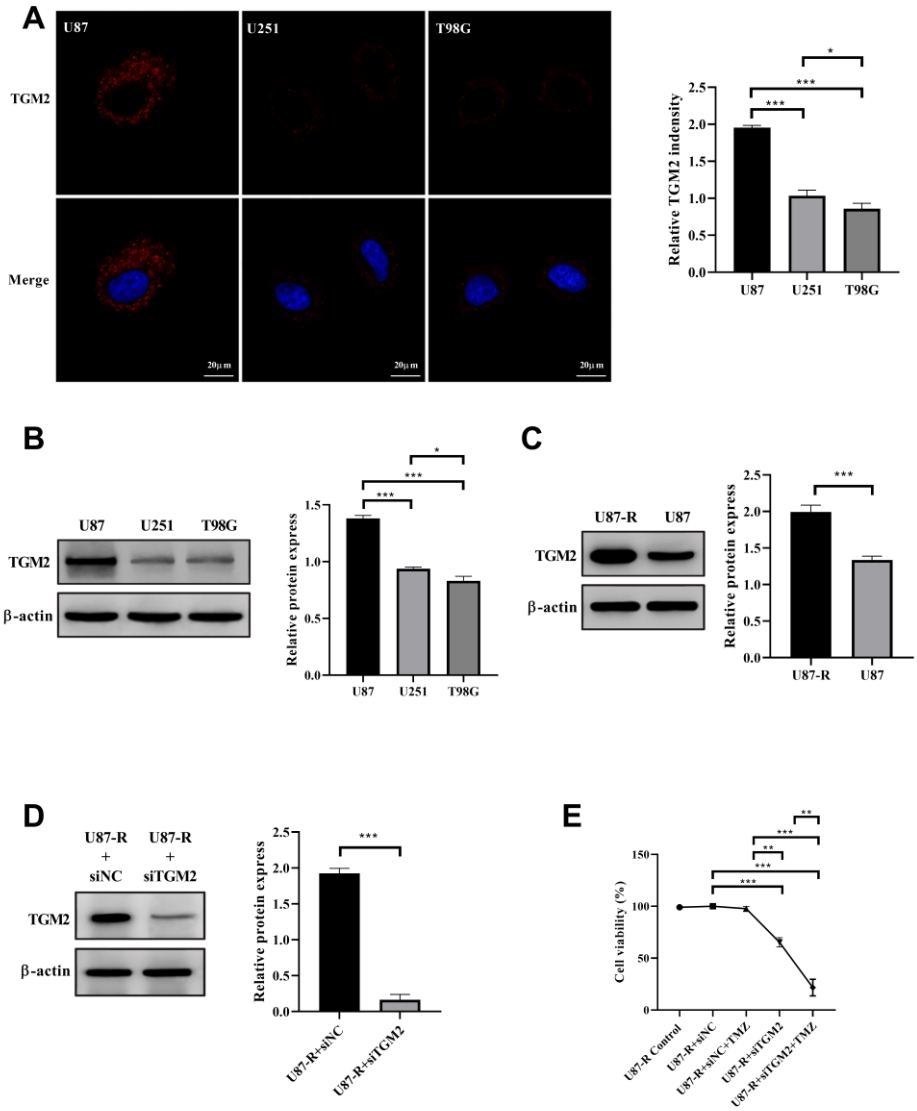

Figure 1: TGM2 is upregulated in glioblastoma cells and contributes to TMZ resistance. (A) Representative immunofluorescence images showing TGM2 expression (red) in U87, U251, and T98G glioblastoma cell lines. Nuclei are counterstained with DAPI (blue). Scale bar: 20 μm. (B) Western blot analysis of TGM2 protein levels in U87, U251, and T98G cells. β-actin served as a loading control. (C) Western blot comparing TGM2 expression between parental U87 cells and TMZ-resistant U87-R cells. (D) Validation of TGM2 knockdown via siRNA in U87-R cells. Western blot shows TGM2 protein levels following transfection with non-targeting control siRNA (si-NC) or TGM2-targeting siRNA (si-TGM2). (E) Cell viability assessed by CCK-8 assay in U87 and U87-R cells treated as indicated. Data are presented as mean ± SEM (n=7 independent experiments). Statistical significance is indicated as *$p < 0.05$, **$p < 0.001$, ***$p < 0.0001$.

In parental U87 cells, cromolyn treatment induced a potent and progressive suppression of cell viability (Figure 2A). The cytotoxic effect became statistically significant at higher concentrations and longer exposures, with 24 h treatment at 8 μM, 16 μM and 32 μM reducing viability by 12.7%, 29.6% and 80.1%, respectively.

This trend culminated in a near-complete ablation of cellular viability after a 72 h exposure to 32 µM cromolyn. Concentration-response modeling yielded progressively lower IC_{50} values of 20.3 µM at 24 h, 13.7 µM at 48 h, and 9.2 µM at 72 h, confirming a clear time-dependent enhancement of potency. A parallel assessment in the TMZ-resistant U87-R cell line revealed a similar qualitative dose- and time-dependent response (Figure 2B); however, a quantitative comparison of the IC_{50} values demonstrated a consistent rightward shift in the resistance curve. The IC_{50} values for U87-R cells were calculated at 25.8 µM (24 h), 19.5 µM (48 h), and 12.4 µM (72 h), all of which are significantly higher than those for the parental line. This concentration- and time-response profiling indicates that while cromolyn exhibits cytotoxic activity against GBM cells, its potency is reduced in the TMZ-resistant subpopulation compared to parental cells. The 95% CIs for cromolyn IC_{50} values were as follows: U87: 24 h (18.7–22.1 µM), 48 h (12.1–15.4 µM), 72 h (8.1–10.4 µM); U87-R: 24 h (23.2–28.6 µM), 48 h (17.4–21.8 µM), 72 h (11.0–13.9 µM).

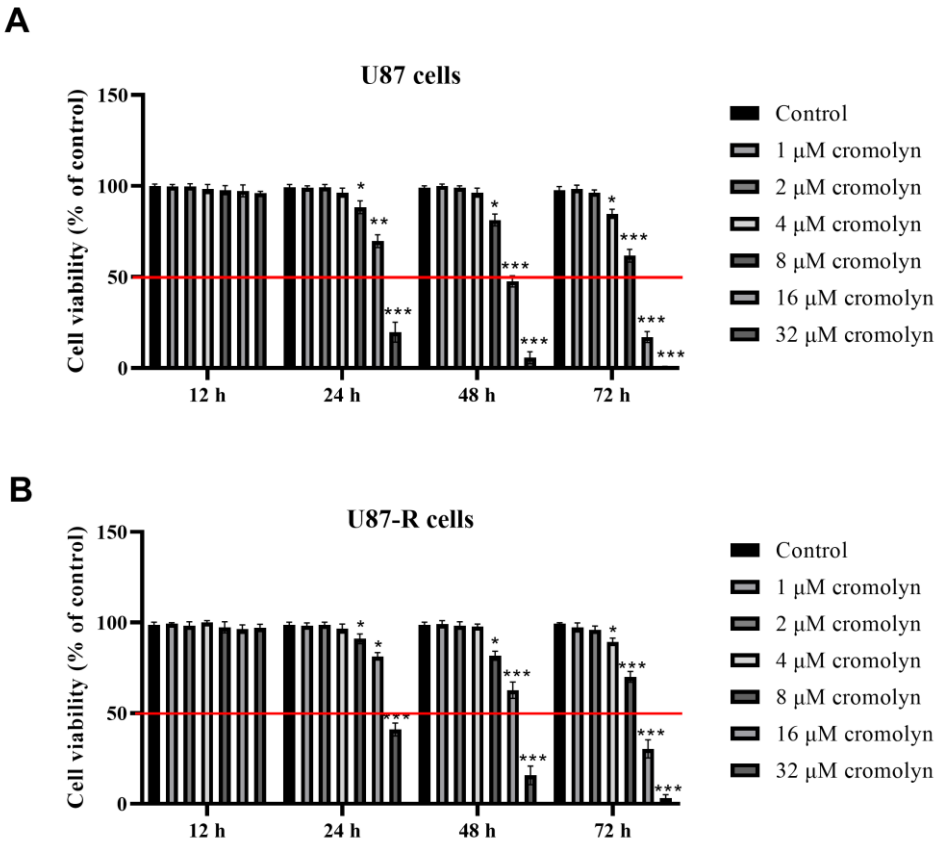

Figure 2: Time- and concentration-dependent effects of cromolyn on the viability of glioblastoma cells. (A) Cell viability of U87 cells and (B) TMZ-resistant U87-R cells following treatment with increasing concentrations of cromolyn (0-32 µM) for 12, 24, 48, and 72 hours, as assessed by CCK-8 assay. Data are presented as mean ± SEM (n=7 independent experiments). * $p < 0.05$, ** $p < 0.001$, *** $p < 0.0001$ vs. respective control (0 µM cromolyn) at each time point.

Cromolyn suppresses TGM2 expression and enhances ferroptotic lipid peroxidation in TMZ-resistant GBM cells

To elucidate the mechanistic basis for cromolyn's action in TMZ-resistant cells, we investigated its capacity to directly modulate TGM2 expression and its functional consequences. Treatment of U87-R cells with a sub-IC_{50} concentration of cromolyn (10 μM) for 24 h resulted in a significant downregulation of TGM2. This suppression was initially visualized by immunofluorescence, which demonstrated a marked reduction in TGM2 staining intensity in TMZ-cromolyn combination groups compared to untreated or TMZ-only groups (Figure 3A and 3B). The qualitative assessment was validated quantitatively by Western blot analysis, which confirmed a substantial decrease in TGM2 protein expression following cromolyn treatment (relative TGM2 band intensity: TMZ = 1.9, TMZ+Cromolyn = 1.1; $p < 0.0001$; Figure 3C). Having established TGM2 as a target, we next probed its functional link to ferroptosis by assessing lipid peroxidation using the C11-$BODIPY^{581/591}$ probe. While TMZ alone or vehicle control failed to induce a significant oxidative shift, treatment with cromolyn, in combination with TMZ, provoked a pronounced oxidation of the sensor, evidenced by a significant increase in the fluorescence shift towards the oxidized (510 nm) state. Quantification revealed an approximately 1.8-fold increase in the mean fluorescence intensity (MIF) of oxidized BODIPY in these groups ($p < 0.0001$; Figure 3D), indicating that cromolyn accelerates lipid peroxidation under these experimental conditions.

Cromolyn enhances ferroptotic vulnerability by suppressing GPX4, inducing ACSL4, and elevating labile iron levels in TMZ-treated cells

Combined TMZ + cromolyn treatment markedly altered cellular redox status, as evidenced by significant GSH depletion and increased lipid peroxidation markers. GSH levels were reduced to 41.3% in TMZ + cromolyn–treated cells compared with the TMZ group ($p < 0.0001$; Figure 4A), and GPX4 levels showed a 54.7% reduction vs. TMZ group ($p < 0.0001$; Figure 4B). Conversely, lipid peroxidation indices were markedly elevated in the combination group: MDA levels increased to 2.35 ± 0.28 nmol compared with 1.15 ± 0.12 nmol in TMZ group ($p < 0.0001$; Figure 4C), and ACSL4 levels rose to 1.8-fold above baseline ($p < 0.0001$; Figure 4D), consistent with enhanced activation of pro-ferroptotic phospholipid remodeling pathways. Importantly, these biochemical changes were largely reversed by ferroptosis inhibitors. Pretreatment with 10 μM Fer-1 or 50 nM Lip-1 partially restored GSH levels to 53.2% and 45.1% of the TMZ-only group, respectively—corresponding to 1.29-fold and 1.09-fold increases relative to the TMZ + cromolyn group ($p < 0.05$ for both), while simultaneously suppressing lipid peroxidation markers (MDA reduced to 1.32 ± 0.19 nmol with Fer-1 and 1.41 ± 0.17 nmol with Lip-1; ACSL4 lowered to 1.1-fold and 1.2-fold, respectively; $p < 0.05$). In contrast, pretreatment with 20 μM Z-VAD or 10 μM Nec-1 failed to rescue GSH or GPX4 depletion and did not reduce MDA or ACSL4 levels ($p > 0.05$ for all comparisons), indicating that neither apoptosis nor necroptosis contributes meaningfully to the cytotoxicity observed. Consistent with these biochemical findings, cromolyn markedly

potentiated TMZ-induced cytotoxicity in U87-R cells; combined TMZ + cromolyn (TMZ 200 μM + cromolyn 10 μM, 24 h) reduced viability by 40.6% vs. TMZ alone ($p < 0.0001$; Figure 4E). Critically, viability was substantially restored by Fer-1 and Lip-1 pretreatment (rescue to 131.6% and 135.1% of the TMZ + cromolyn group, respectively; $p < 0.001$), whereas Z-VAD and Nec-1 produced no significant protection ($p > 0.05$ vs. TMZ + cromolyn). Collectively, these results demonstrate that the enhanced cytotoxicity induced by TMZ + cromolyn co-treatment is mediated predominantly through ferroptosis rather than apoptosis or necroptosis.

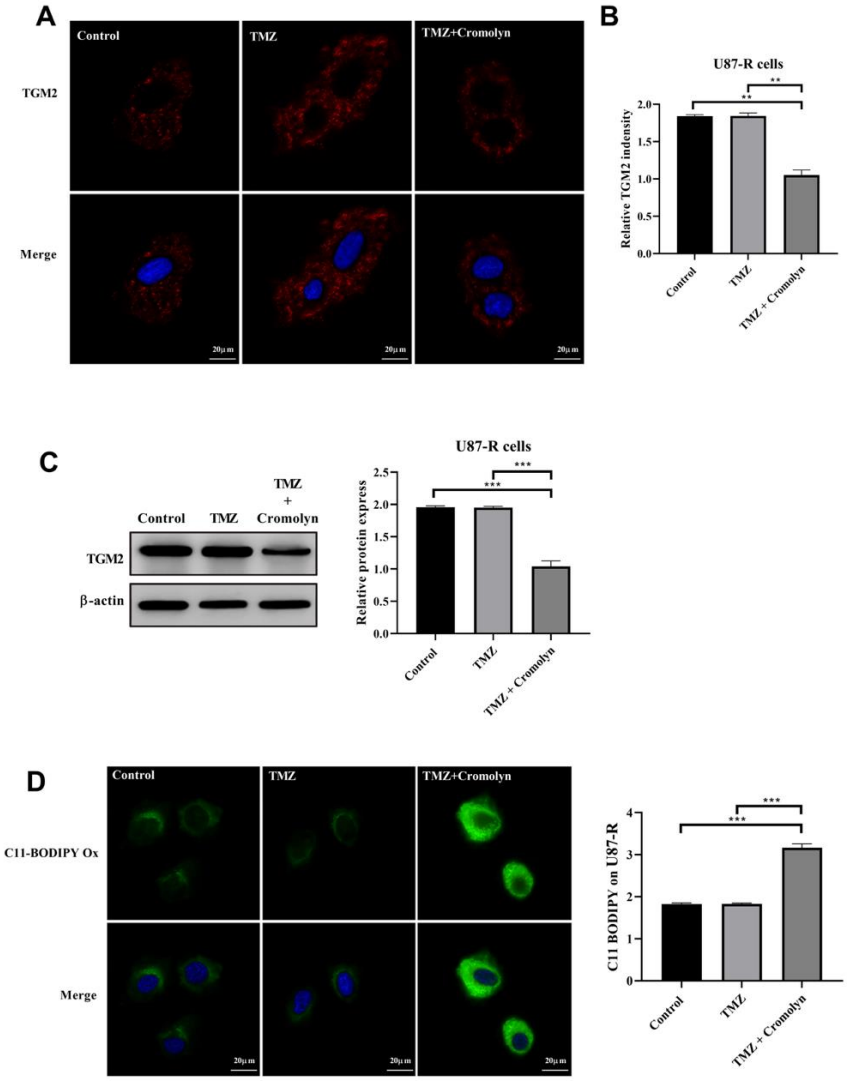

Figure 3: Cromolyn suppressed TGM2 expression and induces lipid peroxidation in TMZ-resistant glioblastoma cells. (A) Representative immunofluorescence images showing TGM2 expression (red) in U87-R cells treated with Control, TMZ alone, or TMZ combined with cromolyn (TMZ+Cromolyn). Nuclei are counterstained with DAPI (blue). Scale bar: 20 μm. (B) Quantitative analysis of the relative TGM2 fluorescence intensity from panel (A). Data are normalized to the control group. (C) Western blot analysis of TGM2 protein expression in U87-R cells under the indicated treatment conditions. β-actin serves as the loading control. (D) Representative fluorescent images of lipid peroxidation detected by C11-BODIPY™ 581/591 staining (oxidized form, green) in U87-R cells. Nuclei are counterstained with DAPI (blue). Scale bar: 20 μm. Quantitative analysis of relative C11-BODIPY oxidation (lipid peroxidation) intensity from panel (D). Data are presented as mean ± SEM (n=7 independent experiments). ** $p < 0.001$, *** $p < 0.0001$

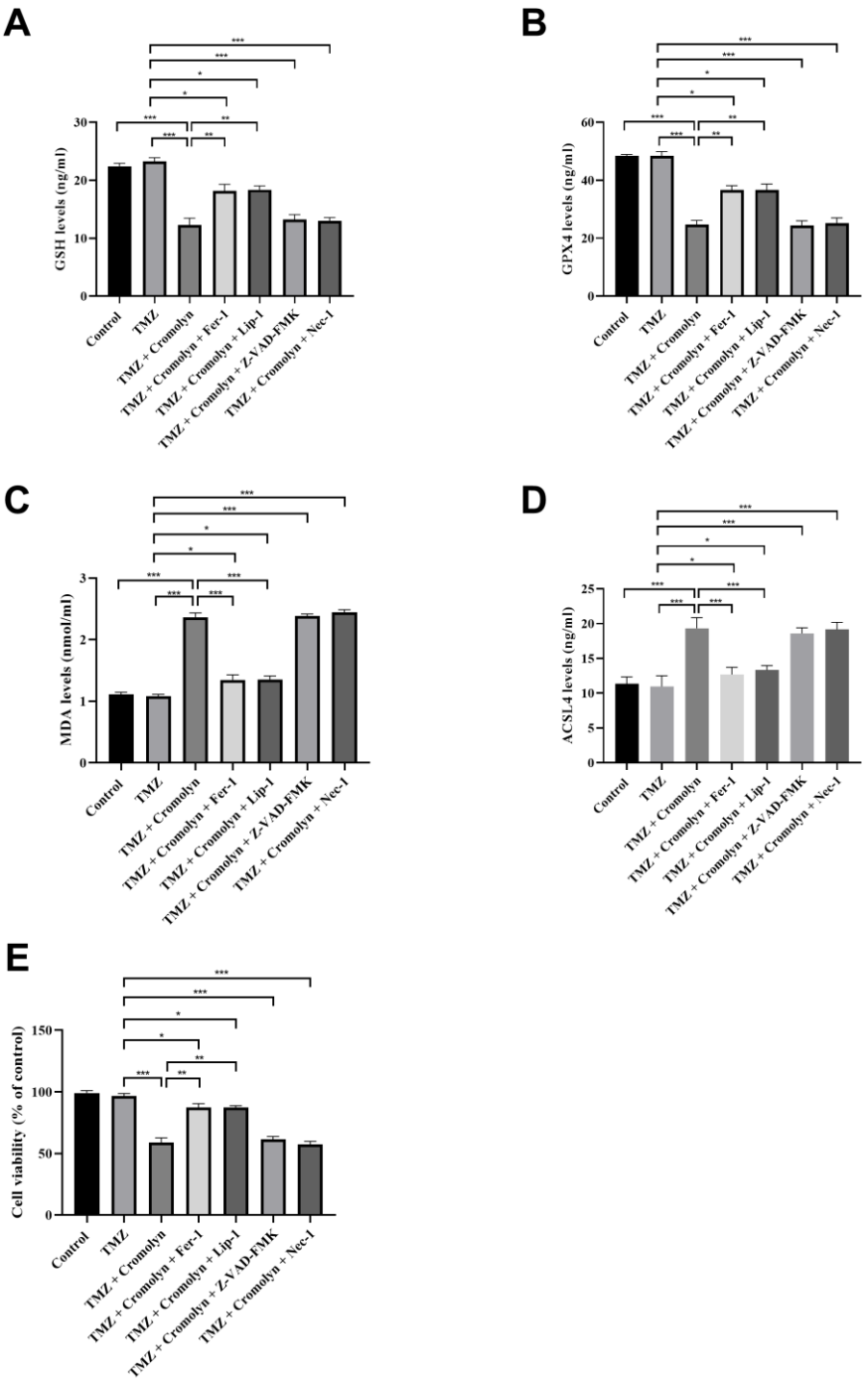

Figure 4: The TMZ and cromolyn combination induces ferroptotic cell death in TMZ-resistant glioblastoma cells. (A) Intracellular GSH levels, (B) GPX4 activity, (C) MDA levels, and (D) ACSL4 levels measured by ELISA in U87-R cells under the indicated treatments. (E) Cell viability assessed by CCK-8 assay in U87-R cells. Treatments include: Control, TMZ alone, TMZ combined with cromolyn (TMZ+Cromolyn), and the combination further treated with the ferroptosis inhibitors Fer-1 (10 μM) or Lip-1 (50 nM), the pan-caspase inhibitor Z-VAD (20 μM), or the necroptosis inhibitor necrostatin-1 (Nec-1, 10 μM). Data are presented as mean ± SEM (n=7 independent experiments). For GSH and viability, values are expressed as fold-change relative to the TMZ + cromolyn group (set to 1.00). * $p < 0.05$, ** $p < 0.001$, *** $p < 0.0001$.

Cromolyn treatment produced reproducible decreases in GPX4 expression and increases in ACSL4 expression relative to untreated controls (GPX4: −56.2%, $p < 0.001$; ACSL4: +82.4%, $p < 0.0001$; Figure 5A and 5B). Consistent with these changes, the labile iron pool was markedly elevated in the TMZ + cromolyn group compared with TMZ alone, as shown by a 2.1-fold increase in FerroOrange fluorescence ($p < 0.0001$; Figure 5C and 5D). Importantly, Deferoxamine (DFO, 10 μM) pretreatment substantially diminished this iron accumulation (FerroOrange reduced to 1.05-fold of TMZ + cromolyn, $p < 0.0001$), confirming that the elevated labile iron is required for the ferroptotic lipid peroxidation signature observed in the combination group.

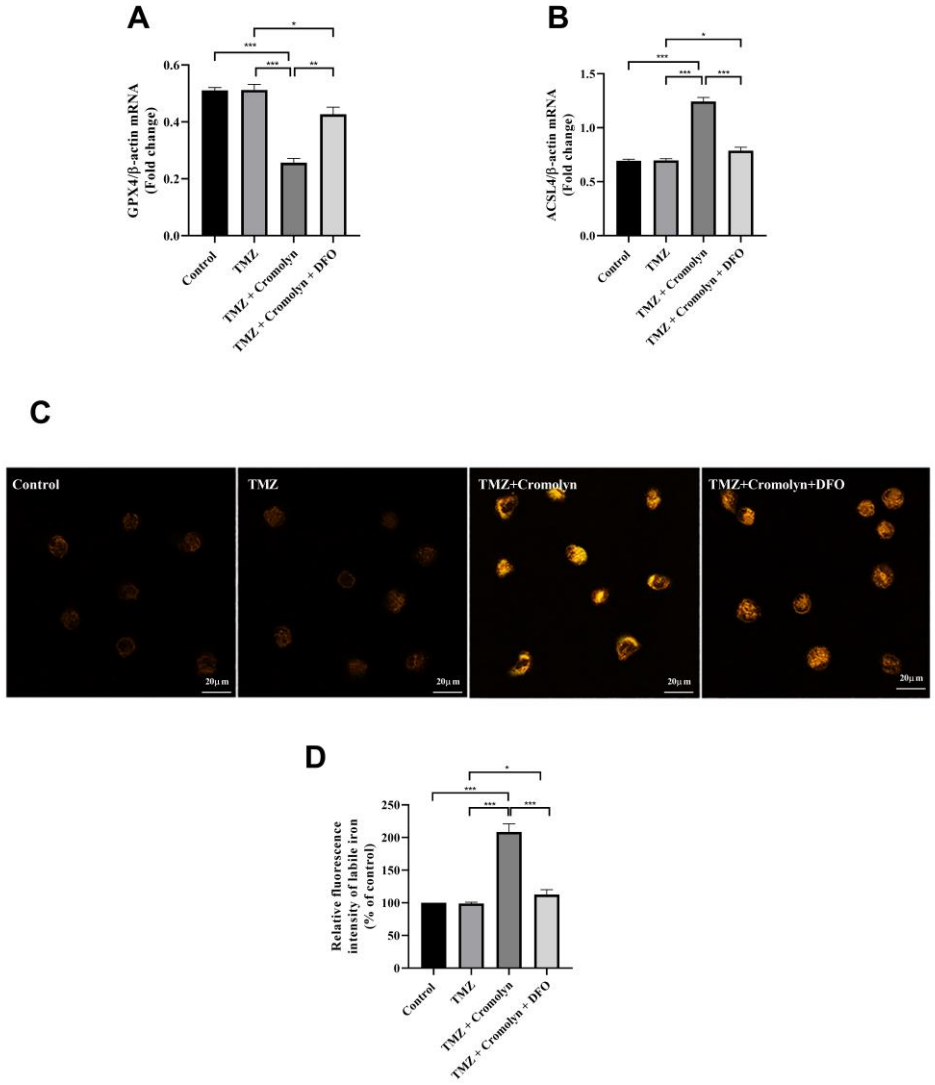

Figure 5: Cromolyn modulated ferroptosis-related gene expression and increase labile iron pool, effects reversed by the iron chelator DFO. (A) Relative mRNA expression of GPX4 and (B) ACSL4 in U87-R cells as determined by RT-qPCR. (C) Representative fluorescent images of labile iron detected by FerroOrange staining in U87-R cells under indicated treatments. Scale bar: 20 μm. (D) Quantitative analysis of relative FerroOrange fluorescence intensity from panel (C), expressed as a percentage of the control. Treatments included: Control, TMZ alone, TMZ combined with cromolyn (TMZ+Cromolyn), and the combination further treated with DFO (10 μM). Data are presented as mean ± SEM (n=7 independent experiments). * $p < 0.05$, ** $p < 0.001$, *** $p < 0.0001$

In parallel, intracellular ROS levels were assessed using the DHE fluorescence assay to further characterize the oxidative landscape associated with ferroptosis. DHE intensity remained low in control and TMZ-only groups, indicating minimal basal superoxide production (Figure 6A and 6B). However, TMZ + cromolyn treatment induced a robust increase in DHE fluorescence, reaching 1.9-fold relative to TMZ alone ($p < 0.0001$), consistent with enhanced oxidative stress. Notably, DFO pretreatment significantly attenuated this elevation, reducing DHE fluorescence to 1.1-fold of the TMZ + cromolyn group ($p < 0.01$), demonstrating that cromolyn-driven superoxide accumulation is also iron dependent.

Notably, MG132 pretreatment (10 μM) partially prevented the cromolyn-mediated downregulation of GPX4 at the mRNA level in the RT-qPCR assay (Figure 6C). GPX4 expression, which was reduced to 51.7% of TMZ group in the TMZ + cromolyn group ($p < 0.0001$), recovered to 48.3% of TMZ + cromolyn in TMZ + cromolyn + MG132 cells ($p < 0.001$), suggesting that post-transcriptional mRNA stabilization, rather than transcriptional activation, may contribute to this recovery. However, given the broad cellular effects of MG132, these results do not definitively establish that cromolyn promotes proteasomal degradation of GPX4. This molecular rescue was mirrored in functional cell viability assays (Figure 6D). While no statistically significant decrease was observed in control or TMZ-only groups, the TMZ + cromolyn combination drastically reduced viability to approximately 42.6% ($p < 0.0001$). Importantly, this loss was significantly attenuated by MG132, with viability in the TMZ + cromolyn + MG132 group showing a 48.4% increase compared to the TMZ + cromolyn group ($p < 0.001$). These molecular alterations are consistent with a mechanistic model in which combined TMZ + cromolyn treatment increases ferroptotic susceptibility in TMZ-resistant GBM cells.

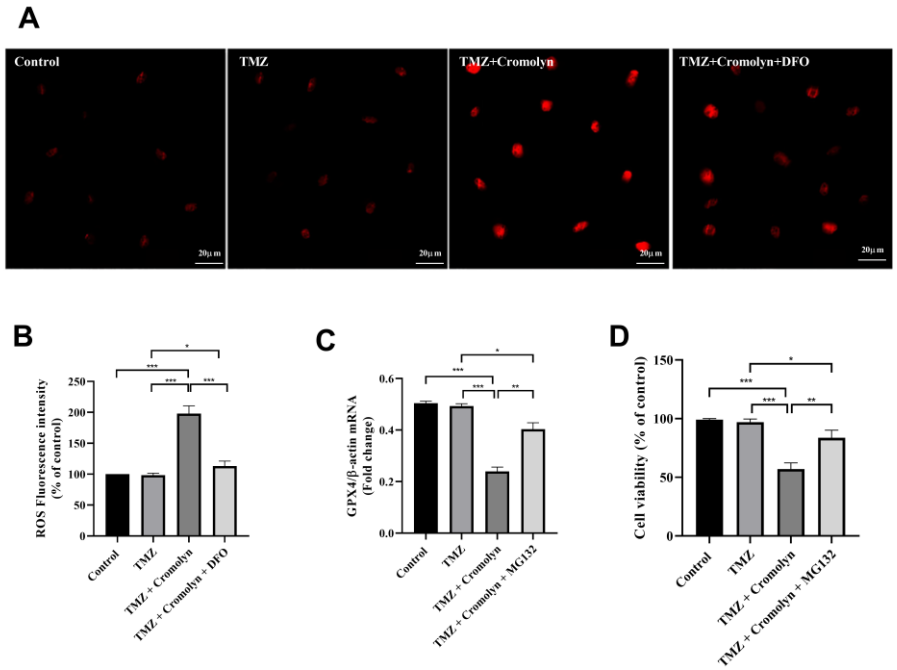

Figure 6: Cromolyn exacerbates TMZ-induced ROS accumulation and GPX4 downregulation, contributing to cell death mitigated by DFO. (A) Representative fluorescent images showing intracellular ROS detected by DHE staining (red) in U87-R cells under the

indicated treatments. Scale bar: 20 μm. (B) Quantitative analysis of relative DHE fluorescence intensity from panel (A). (C) Relative mRNA expression of GPX4 in U87-R cells treated with TMZ and cromolyn, with or without the proteasome inhibitor MG132 (10 μM), as determined by RT-qPCR. (D) Cell viability assessed by CCK-8 assay in U87-R cells. Treatments included: Control, TMZ alone, TMZ combined with cromolyn (TMZ+Cromolyn), and the combination further treated with DFO (10 μM). Data are presented as mean ± SEM (n=7 independent experiments). * $p < 0.05$, ** $p < 0.001$, *** $p < 0.0001$

Discussion

Cromolyn, historically recognized as a mast cell stabilizer, has long been employed in the treatment of allergic asthma and various inflammatory conditions (23). However, an expanding body of evidence now indicates that cromolyn exerts diverse biological functions extending well beyond its classical anti-allergic properties (24). These functions include regulation of microglial signaling, inhibition of cytokine release, modulation of intracellular oxidative stress, and suppression of cancer cell proliferation (25). According to these observations, our study aimed to determine whether cromolyn possesses chemosensitizing properties capable of enhancing the therapeutic efficacy TMZ, the current standard-of-care alkylating agent for GBM. Given that TMZ resistance is a pervasive and clinically significant barrier to effective GBM management (26), the need for adjunct strategies that restore or augment TMZ responsiveness is urgent. Our results demonstrate that cromolyn significantly enhances TMZ-induced cytotoxicity in both TMZ-sensitive U87 and TMZ-resistant U87-R cells, suppresses TGM2 expression at multiple regulatory levels, and triggers a ferroptotic phenotype. Collectively, these findings support the notion that cromolyn warrants further preclinical investigation as a potential adjuvant capable of mitigating chemoresistance in GBM. However, in vivo validation, pharmacokinetic studies, and toxicity assessment are required before any clinical translation can be considered.

The anti-proliferative capacity of cromolyn observed in our study aligns with an increasing number of reports describing its anti-cancer effects in diverse tumor types. Cromolyn has previously been shown to exert potent, dose-dependent growth inhibition in colon, hepatocellular, pancreatic, and cervical carcinoma cell lines, with IC_{50} values generally ranging from low micromolar to sub-micromolar concentrations depending on the exposure duration (18). For example, Motawi et al. reported IC_{50} values between 2–4 μM in HT-29 colon cancer after 72 hours, suggesting that cromolyn may interfere with proliferative pathways broadly across malignancies (27). Supporting these observations, a recent study in breast cancer demonstrated that cromolyn, delivered via chitosan nanoparticles, effectively suppressed tumor growth both in vitro and in vivo by reversing promoter hypermethylation of the tumor-suppressor. Notably, the study utilized cromolyn nanoparticle concentrations between 5–20 μM in breast cancer cell lines, producing marked proliferation arrest and epigenetic reactivation of silenced gene programs (28). Additionally, cromolyn demonstrates relatively low toxicity toward non-malignant cell lines, supporting a favorable therapeutic index (24). In the present study, we extend these findings by demonstrating similar dose- and time-dependent cytotoxic responses in GBM-derived U87 cells, where cromolyn displayed IC_{50}

values of 20.3 μM, 13.7 μM, and 9.2 μM at 24, 48, and 72 hours, respectively. Notably, TMZ-resistant U87-R cells demonstrated higher IC_{50} values (25.8 μM, 19.5 μM, and 12.4 μM), reinforcing the concept that TMZ resistance is accompanied by collateral tolerance to structurally unrelated chemical stressors. Despite this, cromolyn remained cytotoxic and, importantly, enhanced the cytotoxic effects of TMZ at sub-cytotoxic doses—supporting its potential repositioning as a chemotherapy-sensitizing agent rather than a standalone cytotoxic drug. Formal drug interaction modeling (e.g., Bliss independence) was not performed in this study; therefore, the term 'synergy' is not used, and the observed effects are described as enhanced or additive. Regarding the clinical translatability of the concentrations used, it is important to note that while cromolyn sodium has poor oral bioavailability (<1%), alternative routes of administration, such as intranasal or inhaled delivery, have been reported to achieve measurable concentrations in the cerebrospinal fluid (CSF) (29). In clinical trials for Alzheimer's disease, CSF concentrations of cromolyn were considered sufficient to modulate target engagement (19). However, whether similar concentrations can be reliably achieved in the brain tumor microenvironment in humans remains to be determined. The blood–brain barrier (BBB) integrity is also compromised in GBM, which may paradoxically enhance drug delivery but also introduce heterogeneity in local concentrations. Furthermore, the tumor microenvironment may alter cromolyn's pharmacokinetics through altered interstitial fluid pressure and efflux transporter expression. Therefore, the concentration range (0–32 μM) used in this in vitro study should be interpreted as a proof-of-concept, and further pharmacokinetic and biodistribution studies, including convection-enhanced delivery or nanoparticle-based formulations, are required to assess clinical feasibility.

A central mechanistic finding of this work concerns the modulation of TGM2, a multifunctional enzyme implicated in tumor progression, therapeutic resistance, and cell survival pathways across numerous cancers (30). Elevated TGM2 expression has been documented in colorectal, lung, ovarian, and gastric cancers (31-34), where it contributes to increased invasiveness, epithelial–mesenchymal transition, and resistance to chemotherapy or radiotherapy (35,36). In GBM specifically, recent studies have demonstrated that TGM2 promotes DNA damage repair, interacts with p53, modulates autophagy dynamics, and enhances mesenchymal transdifferentiation, thereby contributing to both radioresistance and chemoresistance (26). Notably, strong TGM2 expression correlates with poor prognosis and reduced overall survival among GBM patients. Our findings corroborate and extend these observations by demonstrating that TGM2 is markedly upregulated in TMZ-resistant U87-R cells, and that cromolyn treatment potently reduced TGM2 expression. Downregulation of TGM2 was associated with altered cellular survival and effectively restoring TMZ sensitivity. However, whether TGM2 suppression is the primary mechanism through which cromolyn promotes ferroptosis remains to be established. Future studies incorporating TGM2 overexpression or rescue experiments are warranted to establish causality. In contrast to past reports that primarily linked TGM2 to DNA repair or apoptotic escape, our findings suggest that TGM2 may also influence ferroptotic susceptibility in TMZ-resistant GBM cells. This potential mechanistic link warrants further

investigation in additional models. Although our findings demonstrate that cromolyn markedly suppresses TGM2 expression in TMZ-resistant cells, whether this suppression occurs through direct protein interaction or indirect upstream signaling remains unresolved. Previous studies have consistently shown that cromolyn primarily modulates inflammatory signaling and microglial cytokine release rather than functioning as a classical enzyme inhibitor (16), suggesting a potential upstream regulatory effect on transcriptional pathways such as NF-κB and STAT, both known to drive TGM2 expression in cancer cells (7). Conversely, work in epithelial and breast cancer models shows that small molecules can directly bind the GTP-binding domain of TGM2 and destabilize its active conformation (30, 35), indicating that direct inhibition cannot be fully excluded. To determine whether cromolyn directly targets TGM2 or modulates its expression secondarily through anti-inflammatory signaling, future studies incorporating CETSA, molecular docking, or TGM2 pull-down assays will be essential. Such clarification would refine the mechanistic positioning of cromolyn as either a TGM2-directed therapeutic or a broader ferroptosis-sensitizing agent in GBM.

Ferroptosis, an iron-dependent form of regulated necrosis driven by lipid peroxidation, has emerged as a promising anti-cancer strategy, particularly in malignancies that are refractory to apoptosis-based therapies (37). GBM cells are characterized by metabolic plasticity, disrupted redox homeostasis, and intrinsic resistance to mitochondrial apoptotic pathways, making ferroptosis an attractive alternative mechanism of tumor cell elimination (38). Previous studies have shown that GBM cells exhibit sensitivity to GPX4 inhibition, and that enhancing ACSL4 expression or lipid ROS accumulation can promote ferroptosis (39,40). In parallel, ferroptosis has recently been described in microglial cells treated with cromolyn, where NCOA4-dependent ferritinophagy was shown to amplify iron-dependent oxidative stress (24). Our findings significantly extend these insights to GBM for the first time. We demonstrate that TMZ + cromolyn co-treatment leads to profound GSH depletion, downregulation of GPX4, upregulation of ACSL4, and increases in MDA, consistent with a ferroptotic signature. Moreover, labile iron pools, assessed via FerroOrange fluorescence, were markedly elevated and largely reversed by DFO chelation, supporting the iron dependence of the observed lipid peroxidation. Ferroptosis inhibitors Fer-1 and Lip-1 restored cell viability, whereas apoptosis and necroptosis inhibitors did not. Taken together, the combination of lipid peroxidation, iron dependence, and pharmacological rescue by ferroptosis inhibitors, but not by apoptosis or necroptosis inhibitors, provides strong evidence that the observed cytotoxicity is mediated predominantly through ferroptosis. However, no single marker alone is sufficient to definitively establish ferroptosis, and our conclusion is based on the convergence of multiple lines of evidence. Compared with previous ferroptosis studies in GBM, the unique observation that cromolyn enhances TMZ-induced ferroptosis introduces a novel drug combination strategy with substantial translational potential.

The relationship between TGM2 and ferroptosis represents a particularly intriguing mechanistic axis. Recent knockout studies have suggested that loss of TGM2 confers relative resistance to ferroptosis induced by RSL3 and erastin, despite paradoxically reduced GPX4 expression, indicating a more complex regulatory network involving

iron metabolism and lipid homeostasis (41). This apparent paradox may be resolved by distinguishing between chronic genetic ablation and acute pharmacological inhibition. Chronic TGM2 knockout triggers compensatory adaptive mechanisms, including altered iron metabolism and lipid remodeling, that ultimately confer resistance despite a pro-ferroptotic baseline profile. In contrast, acute pharmacological inhibition (cromolyn, 24 h) may not permit sufficient time for such compensatory adaptation to emerge. Mechanistically, a recent study revealed that TGM2 directly serotonylates GPX4 at Gln55 and Gln77, enhancing GPX4 protein stability and thereby conferring ferroptosis resistance. Consequently, inhibiting TGM2 activity is expected to destabilize GPX4 and sensitize cells to ferroptosis, precisely the phenotype observed in our study. Thus, our data are mechanistically concordant with the emerging model that TGM2 activity promotes ferroptosis resistance, while chronic TGM2 deletion triggers complex compensatory rewiring that obscures this relationship. In the present study, we show that pharmacologic inhibition of TGM2 through cromolyn sensitizes GBM cells to ferroptotic death, increases lipid ROS accumulation, and elevates iron availability. Additionally, MG132 rescue experiments are consistent with the possibility that cromolyn-mediated GPX4 suppression may partly involve proteasomal degradation pathways. However, MG132 has broad cellular effects, including modulation of oxidative stress and protein homeostasis, and our data do not provide direct evidence of altered GPX4 ubiquitination or protein stability. Therefore, this mechanism remains speculative and requires further investigation using direct assays of GPX4 ubiquitination and stability. It is important to note that MG132 may also indirectly stabilize GPX4 mRNA through p38 MAPK-dependent inhibition of mRNA degradation, as demonstrated for other transcripts in cancer cells. This does not imply transcriptional activation but rather post-transcriptional mRNA stabilization, which is consistent with the partial recovery of GPX4 mRNA levels observed in our RT-qPCR analysis. This supports a model in which TGM2 functions as a central regulator of redox and lipid metabolic programs, facilitating resistance to ferroptosis in TMZ-resistant GBM cells. By disrupting TGM2 function, cromolyn effectively dismantles a key molecular barrier to ferroptotic engagement, providing a unified mechanistic explanation for the enhanced TMZ sensitivity observed in our study. Despite the compelling mechanistic and translational insights provided by this study, several limitations should be considered when interpreting the present findings. First, all experiments were conducted in established glioblastoma cell lines (U87, U251, T98G) and a TMZ-resistant derivative generated in vitro using our previously validated protocol (22). While both this study and our prior work share the U87-R model, they focus on distinct molecular axes, Notch1/MVP in the former and TGM2/ferroptosis in the present study, with the current work uniquely implicating TGM2 as a regulator of ferroptotic sensitivity in TMZ-resistant GBM. While this approach enables mechanistic dissection, it does not fully recapitulate the cellular heterogeneity, three-dimensional architecture, or metabolic gradients of patient tumors. Future studies using patient-derived GBM cells, organoid models, and in vivo xenograft systems will be essential to validate the translational relevance of our observations. Second, although we demonstrate that cromolyn downregulates TGM2 expression and promotes ferroptosis, the precise molecular interaction between

cromolyn and TGM2 remains unresolved. Whether cromolyn directly binds TGM2 or acts through upstream signaling pathways (e.g., NF-κB or STAT) requires further investigation using methods such as cellular thermal shift assays (CETSA), molecular docking, or pull-down assays. Third, the pharmacokinetic properties of cromolyn, particularly its ability to cross the blood–brain barrier (BBB) and achieve sufficient concentrations in the brain tumor microenvironment, have not been directly addressed in this study. While intranasal or inhaled delivery has been explored in other neurological conditions, the extent to which these routes yield therapeutic levels in GBM patients remains unknown. Fourth, our study focused on short-term (up to 72 hours) cytotoxic and ferroptotic effects. The long-term consequences of combined TMZ and cromolyn treatment, including potential adaptive resistance mechanisms or effects on non-malignant brain cells (e.g., astrocytes, microglia), were not evaluated. Fifth, the fluorescence microscopy analyses of labile iron (FerroOrange; Figure 5C–D) and ROS (DHE; Figure 6A–B) were performed without nuclear counterstaining. While acquisition parameters were strictly standardized across all conditions and cells were seeded at identical densities, we acknowledge that treatment-induced differences in cell density could influence the measured fluorescence intensities. Future studies incorporating nuclear normalization (e.g., DAPI co-staining) would provide more rigorous per-cell quantification and are warranted to validate our findings. Sixth, although we demonstrate that TGM2 knockdown increases TMZ sensitivity and that cromolyn reduces TGM2 expression while promoting ferroptosis, we did not perform TGM2 overexpression/rescue experiments to establish that TGM2 suppression is the causal mechanism through which cromolyn promotes ferroptosis. Future studies incorporating TGM2 overexpression or rescue experiments are warranted to establish causality. Additionally, whether TGM2 knockdown reproduces the full ferroptotic phenotype induced by cromolyn, including changes in lipid peroxidation, GPX4, ACSL4, and labile iron, remains to be determined. Seventh, although three GBM cell lines (U87, U251, T98G) were initially screened, the major mechanistic experiments were conducted primarily in U87 and its TMZ-resistant derivative U87-R. This limits the generalizability of our findings given the well-established molecular heterogeneity of GBM. Future studies validating the principal findings, particularly cromolyn/TMZ sensitization and ferroptosis-related effects, in additional GBM models, preferably another TMZ-resistant model, are warranted. Until such validation is performed, our conclusions should be considered specific to the U87/U87-R model. Finally, the immunomodulatory effects of cromolyn-induced ferroptosis in the GBM microenvironment were not examined. Given the emerging role of ferroptosis in regulating anti-tumor immunity, future studies should specifically address two major translational barriers: (i) whether cromolyn can reach therapeutic concentrations in the GBM tumor microenvironment across an intact or disrupted blood–brain barrier, using clinically relevant delivery routes; and (ii) how cromolyn and TMZ co-treatment affects the complex immune landscape of GBM, including tumor-associated macrophages and ferroptosis-driven immunogenicity.

Conclusions

In conclusion, our findings suggest a previously underexplored role for cromolyn in sensitizing TMZ-resistant glioblastoma cells to chemotherapy in vitro. By suppressing TGM2 expression and promoting ferroptosis-associated lipid peroxidation, cromolyn may represent a candidate for further preclinical investigation as an adjuvant in GBM treatment. However, in vivo efficacy, pharmacokinetic properties, and safety profiles remain to be established, and no clinical applicability can be claimed at this stage.

Conflict of interest: The authors declare no conflict interest.
Funding source: The authors declare that no financial support was received for the research.
Ethical approval: Ethical approval is not applicable to this study, as it solely involved in vitro experiments with cell cultures, without the use of human or animal subjects or tissues.
Informed consent: Not applicable
Acknowledgments: None.
Peer-review: Externally. Evaluated by independent reviewers working in at least two different institutions appointed by the field editor.
Data availability: The data supporting the results of this study are available from the corresponding author upon reasonable request.
Contributions:
Research concept and design: CH, AK, BO
Data analysis and interpretation: CH, AK, BO
Data collection and/or assembly of data: CH, AK, BO
Writing the article: CH, AK, BO
Critical revision of the article: CH, AK, BO
Final approval of the article: CH, AK, BO
All authors read and approved the final version of the manuscript.

References

1. Qi Y, Liu B, Sun Q, Xiong X, Chen Q. Immune checkpoint targeted therapy in glioma: status and hopes. Front Immunol. 2020;11:578877.
2. Hu Z, Mi Y, Qian H, Guo N, Yan A, Zhang Y,et al. A potential mechanism of temozolomide resistance in glioma-ferroptosis. Front Oncol. 2020;10:897.
3. Brennan CW, Verhaak RG, McKenna A, Campos B, Noushmehr H, Salama SR,et al. The somatic genomic landscape of glioblastoma. Cell. 2013;155(2):462-77.
4. Wu Y, Song Y, Wang R, Wang T. Molecular mechanisms of tumor resistance to radiotherapy. Mol Cancer. 2023;22(1):96.
5. Fésüs L, Szondy Z. Transglutaminase 2 in the balance of cell death and survival. FEBS Lett. 2005;579(15):3297-302.
6. Tóth B, Garabuczi E, Sarang Z, Vereb G, Vámosi G, Aeschlimann D, et al. Transglutaminase 2 is needed for the formation of an efficient phagocyte portal in macrophages engulfing apoptotic cells. J Immunol. 2009;182(4):2084-92.
7. Yin J, Oh YT, Kim JY, Kim SS, Choi E, Kim TH, et al. Transglutaminase 2 inhibition reverses mesenchymal transdifferentiation of glioma stem cells by regulating C/EBPβ signaling. Cancer Res. 2017;77(18):4973-84.
8. Tucholski J. TG2 protects neuroblastoma cells against DNA-damage-induced stress, suppresses p53 activation. Amino Acids. 2010;39(2):523-32.
9. Gundemir S, Monteagudo A, Akbar A, Keillor JW, Johnson GVW. The complex role of transglutaminase 2 in glioblastoma proliferation. Neuro Oncol. 2017;19(2):208-18.

10. Dixon SJ, Lemberg KM, Lamprecht MR, Skouta R, Zaitsev EM, Gleason CE, et al. Ferroptosis: an iron-dependent form of nonapoptotic cell death. Cell. 2012;149(5):1060-72.
11. Carlos A, Mendes M, Cruz MT, Pais A, Vitorino C. Ferroptosis driven by nanoparticles for tackling glioblastoma. Cancer Lett. 2024;611:217392.
12. Hangauer MJ, Viswanathan VS, Ryan MJ, Bole D, Eaton JK, Matov A, et al. Drug-tolerant persister cancer cells are vulnerable to GPX4 inhibition. Nature. 2017;551(7679):247-50.
13. Lei G, Zhang Y, Koppula P, Liu X, Zhang J, Lin SH, et al. The role of ferroptosis in ionizing radiation-induced cell death and tumor suppression. Cell Res. 2020;30(2):146-62.
14. Mao Z, Hu Y, Zhao Y, Zhang X, Guo L, Wang X,et al. The mutual regulatory role of ferroptosis and immunotherapy in anti-tumor therapy. Apoptosis. 2024;29(9-10):1291-308.
15. Gagliardi M, Saverio V, Rossin F, D'Eletto M, Corazzari M. Transglutaminase 2 and ferroptosis: a new liaison? Cell Death Discov. 2023;9(1):88.
16. Wang YJ, Monteagudo A, Downey MA, Ashton-Rickardt PG, Elmaleh DR. Cromolyn inhibits the secretion of inflammatory cytokines by human microglia (HMC3). Sci Rep. 2021;11(1):8054.
17. Arumugam T, Ramachandran V, Logsdon CD. Effect of cromolyn on S100P interactions with RAGE and pancreatic cancer growth and invasion in mouse models. J Natl Cancer Inst. 2006;98(24):1806-18.
18. Motawi TM, Bustanji Y, El-Maraghy S, Taha MO, Al-Ghussein MA. Evaluation of naproxen and cromolyn activities against cancer cell viability, proliferation, apoptosis, p53 and gene expression of survivin and caspase-3. J Enzyme Inhib Med Chem. 2014;29(2):153-61.
19. Zhang C, Griciuc A, Hudry E, Wan Y, Quinti L, Ward J, et al. Cromolyn reduces levels of the Alzheimer's disease-associated amyloid β-protein by promoting microglial phagocytosis. Sci Rep. 2018;8(1):1144.
20. Hori Y, Takeda S, Cho H, Wegmann S, Shoup TM, Takahashi K, et al. A Food and Drug Administration-approved asthma therapeutic agent impacts amyloid β in the brain in a transgenic model of Alzheimer disease. J Biol Chem. 2015;290(4):1966-78.
21. Wang YJ, Downey MA, Choi S, Shoup TM, Elmaleh DR. Cromolyn platform suppresses fibrosis and inflammation, promotes microglial phagocytosis and neurite outgrowth. Sci Rep. 2021;11(1):22161.
22. Tuncer C, Hacioglu C. Notch1 and major vault proteins modulate temozolomide resistance in glioblastoma. J Cell Mol Med. 2025;29(6):e70474.
23. Storms W, Kaliner MA. Cromolyn sodium: fitting an old friend into current asthma treatment. J Asthma. 2005;42(2):79-89.
24. Kilic M, Hacioglu C, Tuncer S, Taskesen A, Tuncer C. Ferroptosis-inducing effects of cromolyn in microglia through NCOA4-mediated ferritinophagy. Metab Brain Dis. 2025;40(8):304.
25. Wang YJ, Downey MA, Choi S, Shoup TM, Elmaleh DR. Cromolyn platform suppresses fibrosis and inflammation, promotes microglial phagocytosis and neurite outgrowth. Sci Rep. 2021;11(1):22161.
26. Sun C, Du Z, Yang W, Wang Q. Transglutaminase 2 nuclear localization enhances glioblastoma radiation resistance. Discov Oncol. 2025;16(1):952.
27. Motawi TK, El-Maraghy SA, ElMeshad AN, Nady OM, Hammam OA. Cromolyn chitosan nanoparticles as a novel protective approach for colorectal cancer. Chem Biol Interact. 2017;275:1-12.
28. Motawi TK, El-Maraghy SA, Sabry D, Nady OM, Senousy MA. Cromolyn chitosan nanoparticles reverse the DNA methylation of RASSF1A and p16 genes and mitigate DNMT1 and METTL3 expression in breast cancer cell line and tumor xenograft model in mice. Chem Biol Interact. 2022;365:110094.
29. Brazier D, Perry R, Keane J, Barrett K, Elmaleh DR. Pharmacokinetics of Cromolyn and Ibuprofen in Healthy Elderly Volunteers. Clin Drug Investig. 2017;37(11):1025-34.
30. Kuo TF, Tatsukawa H, Kojima S. New insights into the functions and localization of nuclear transglutaminase 2. FEBS J. 2011;278(24):4756-67.

31. Malkomes P, Lunger I, Oppermann E, Lorenz J, Faqar-Uz-Zaman SF, Han J, et al. Transglutaminase 2 is associated with adverse colorectal cancer survival and represents a therapeutic target. Cancer Gene Ther. 2023;30(10):1346-54.
32. Zhang L, Li Q, Yang J, Xu P, Xuan Z, Xu J, et al. Cytosolic TGM2 promotes malignant progression in gastric cancer by suppressing TRIM21-mediated ubiquitination/degradation of STAT1 in a GTP binding-dependent modality. Cancer Commun. 2023;43(1):123-49.
33. Cao L, Petrusca DN, Satpathy M, Nakshatri H, Petrache I, Matei D. Tissue transglutaminase protects epithelial ovarian cancer cells from cisplatin-induced apoptosis by promoting cell survival signaling. Carcinogenesis. 2008;29(10):1893-900.
34. Huaying S, Dong Y, Chihong Z, Xiaoqian Q, Danying W, Jianguo F. Transglutaminase 2 inhibitor KCC009 induces p53-independent radiosensitization in lung adenocarcinoma cells. Med Sci Monit. 2016;22:901605.
35. Kumar A, Xu J, Sung B, Kumar S, Yu D, Aggarwal BB, et al. Evidence that GTP-binding domain but not catalytic domain of transglutaminase 2 is essential for epithelial-to-mesenchymal transition in mammary epithelial cells. Breast Cancer Res. 2012;14(1):R4.
36. Aepler J, Wodtke J, Wodtke R, Haase-Kohn C, Loser R, Pietzsch J, et al. The role of transglutaminase 2 in the radioresistance of melanoma cells. Cells. 2022;11(8):1342.
37. Lei G, Zhuang L, Gan B. Targeting ferroptosis as a vulnerability in cancer. Nat Rev Cancer. 2022;22(7):381-96.
38. Singh S, Mohapatra I, Barik D, Zheng H, Kim S, Sharma M, et al. Harnessing ferroptosis to transform glioblastoma therapy and surmount treatment resistance. Cell Death Discov. 2025;11(1):448.
39. Zhuo S, He G, Chen T, Li X, Liang Y, Wu W, et al. Emerging role of ferroptosis in glioblastoma: therapeutic opportunities and challenges. Front Mol Biosci. 2022;9:974156.
40. Kilic G, Hacioglu C, Tuncer C, Kar E, Kar F, Taskesen A, et al. Boric acid suppresses glioblastoma cellular survival by regulating ferroptosis via SOX10/GPx4/ACSL4 signalling and iron metabolism. J Cell Mol Med. 2025;29(7):e70529.
41. Gagliardi M, Saverio V, Rossin F, D'Eletto M, Corazzari M. Transglutaminase 2 and ferroptosis: a new liaison? Cell Death Discov. 2023;9(1):88.

Publisher's Note: Unico's Medicine remains neutral with regard to jurisdictional claims in published maps and institutional affiliations.